



Increasing wintertime ozone levels and secondary aerosol formation in the Guanzhong basin, central China

Tian Feng ^{a,c,*}, Shuyu Zhao ^b, Xiu Zhang ^a, Qiyuan Wang ^b, Lang Liu ^b, Guohui Li ^b, Xuexi Tie ^b

^a Department of Geography & Spatial Information Techniques, Ningbo University, Ningbo, Zhejiang 315211, China

^b Key Lab of Aerosol Chemistry and Physics, SKLQO, Institute of Earth Environment, Chinese Academy of Sciences, Xi'an, Shaanxi 710061, China

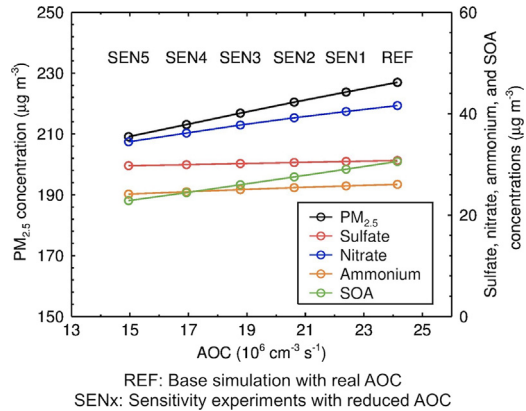
^c Institute of East China Sea, Ningbo University, Ningbo, Zhejiang 315211, China



HIGHLIGHTS

- The ozone level has increased remarkably in GZB, showing enhanced AOC.
- The population hourly and postmeridian Ox concentrations trace the AOC well.
- The AOC change affects the secondary aerosol formation, especially SOA and nitrate.

GRAPHICAL ABSTRACT



ARTICLE INFO

Article history:

Received 25 May 2020

Received in revised form 9 July 2020

Accepted 12 July 2020

Available online 20 July 2020

Editor: Jianmin Chen

Keywords:

Ozone

Atmospheric oxidizing capacity

Secondary aerosols

WRF-Chem

ABSTRACT

The observed near-surface ozone (O_3) concentration has been remarkably increasing during recent years in winter in the Guanzhong basin, central China, showing a continuous enhancement of the atmospheric oxidizing capacity (AOC). The impact of such a change in the AOC on secondary aerosol formation, however, has not yet been assessed. In this study, we simulate the formation of O_3 and airborne particles in the atmosphere using the WRF-Chem model, in which the AOC is calculated quantitatively, to understand the responses of secondary aerosols to the AOC increase. Meteorological observations, air pollutants including O_3 , NO_2 , SO_2 , CO , and $\text{PM}_{2.5}$ concentrations at ambient monitoring sites, and the main compositions of submicron particulates measured using ACSM are used to constrain the model simulation. The model result shows that the population hourly and postmeridian $\text{O}_x (= \text{O}_3 + \text{NO}_2)$ concentrations are good indicators for the wintertime AOC in the basin, suggested by the significantly positive correlations between them. Sensitivity experiments present that the AOC changes may exert important influences on fine particle ($\text{PM}_{2.5}$) concentration with an average rate of $1.94 (\mu\text{g m}^{-3}) / (10^6 \text{ cm}^{-3} \text{ s}^{-1})$ for $\Delta(\text{PM}_{2.5}) / \Delta(\text{AOC})$, which is mostly caused by the mass changes in secondary organic aerosol (43%) and nitrate aerosol (40%) and less attributed to the ammonium (11%) and sulfate (6%) components.

© 2020 Published by Elsevier B.V.

1. Introduction

The haze pollution with high levels of fine particle ($\text{PM}_{2.5}$) or aerosol concentration has frequently occurred in eastern and central China

* Corresponding author at: Department of Geography & Spatial Information Techniques, Ningbo University, Ningbo, Zhejiang 315211, China.

E-mail address: fengtian@nbu.edu.cn (T. Feng).

during recent years, particularly in winter (Bei et al., 2016a,b; Feng et al., 2018; Zhao et al., 2015). A large mass loading of PM_{2.5} not only deteriorates air quality and visibility (Cao et al., 2012a; Feng et al., 2016b; Seinfeld and Pandis, 2006), but also threatens human health and the ecosystem (Cao et al., 2012b; Tie et al., 2016). Additionally, the existence of aerosol can affect the energy budget of the earth via absorbing and scattering the solar radiation and also serving as cloud condensation nuclei and ice nuclei which alter cloud albedo and lifetime (Li et al., 2008, 2009; Zhou et al., 2017).

Among the chemical species in PM_{2.5}, secondary aerosols including secondary organic aerosol (SOA) and inorganic components such as sulfate, nitrate, and ammonium account for dominating fractions of the total mass concentration (Feng et al., 2016b, 2018; Li et al., 2017a; L. Liu et al., 2019). These secondary aerosols are usually formed through gas-phase oxidation reactions participated by oxidants including hydroxyl radical (OH), O₃, and nitrate radical (NO₃), and gas-particle partitioning processes in the atmosphere (Kim et al., 2014; Odum et al., 1996; Seinfeld and Pandis, 2006; Tsimpidi et al., 2010). For example, SOA is produced in the oxidation of precursors including volatile organic compounds (VOCs) from natural and anthropogenic sources (Odum et al., 1996; Pankow, 1994), evaporated organic gases from primary organic aerosol (POA), and intermediate VOCs (IVOCs) co-emitted with POA (Lipsky and Robinson, 2006; Robinson et al., 2007; Srivastava et al., 2008; Tsimpidi et al., 2010). Nitrate aerosol is formed via the balance of nitric acid (HNO₃) with inorganic cations in aerosol, ammonium for most cases. In ambient air, HNO₃ is generated in the homogeneous and heterogeneous conversions of N₂O₅ and the gas-phase reactions including NO₂ reaction with OH and NO₃ radical reaction with hydrocarbons (Kim et al., 2014; L. Liu et al., 2019). The oxidation rates of these gas-phase reactions depend on the abundance of oxidants in the atmosphere and hence are closely associated with the atmospheric oxidizing capacity (AOC) (Feng et al., 2019; Tsimpidi et al., 2010).

As the most important oxidant in the atmosphere, OH radical removes most of the trace gases through oxidizing processes (Elshorbany et al., 2009; Stone et al., 2012). OH radical originates from the reaction of excited atomic oxygen (O¹D) with H₂O, the reactions of hydroperoxyl radical (HO₂) with NO and O₃, the reactions of unsaturated hydrocarbons with O₃, and the photolysis of nitrous acid (HONO), hydrogen peroxide (H₂O₂), and oxygenated VOCs (OVOCs) (Elshorbany et al., 2009; Lelieveld et al., 2016). Field campaigns have been performed to investigate the radical chemistry of the atmosphere

(Elshorbany et al., 2009; Fuchs et al., 2017; Ren et al., 2006; Sheehy et al., 2010; Stone et al., 2012; Tan et al., 2017). Rohrer et al. (2014) have studied the OH chemistry at different kinds of stations regarding air pollution. However, due to the complexity in the measuring instrument and techniques, it is not easy to obtain OH radical concentrations. By comparison, ambient O₃ concentration is much easier to measure and often used as an indicator to trace the AOC level (Liu et al., 1988).

In China, the observed surface O₃ concentration has been increasing significantly during recent years (Cheng et al., 2016; Gao et al., 2017; Li et al., 2017b; Liu et al., 2019; Lu et al., 2018; Ma et al., 2016; Sun et al., 2016). Gao et al. (2017) have observed a long-term increase in O₃ concentration of 1.1 ppb yr⁻¹ from 2006 to 2015 in Shanghai, China. In Beijing and surrounding areas, similar increases have been also found in the measured daily maximum 1 h O₃ concentration (1.8 ppb yr⁻¹, urban and 2.1 ppb yr⁻¹, background) and daily maximum 8 h O₃ (MDA8 O₃) concentration (1.1 ppb yr⁻¹, Shangdianzi, rural) during the past decade (Cheng et al., 2016; Ma et al., 2016). At a regional background site over Mount Tai, the measured O₃ concentration has increased by 1.7 ppb yr⁻¹ for June and 2.1 ppb yr⁻¹ for June–August from 2003 to 2015 (Sun et al., 2016). Recently, Lu et al. (2018) have reported that the measured O₃ concentration shows a continuous increase from 2013 to 2017 during the warm season (April–September) averaged over the 74 cities of China, and the largest increases in ozone exposure are in eastern and central China. The MDA8 O₃ concentration over north China has also increased with a rate of 7.9 µg m⁻³ yr⁻¹ from 2013 to 2017 during April–October (J. Liu et al., 2019). Such increases in surface O₃ concentration suggest an enhancement of the AOC over China (Liu et al., 1988), which potentially facilitate the formation of secondary aerosols (Feng et al., 2019; Wang et al., 2016).

The Guanzhong basin (GZB), located in central China, also suffers severe O₃ and haze pollutions during recent years (Feng et al., 2016a, b, 2018; Li et al., 2018). Feng et al. (2016a) have reported a severe complex air pollution in August 2013 in Xi'an, the largest city in the basin, where the maximal O₃ and PM_{2.5} concentrations reach around 225 µg m⁻³ and 180 µg m⁻³. From 2013 to 2019, the observed wintertime O₃ concentration presents a significant increase in the basin as described in Section 3.1, indicating an enhancement of the AOC. However, the effects of the increasing O₃ level as well as the AOC on PM_{2.5} concentration in the basin, particularly on the formation of secondary aerosols in airborne particles has not yet been evaluated. In this study, we assess the impacts of the increasing AOC on wintertime secondary aerosol formation in GZB using the

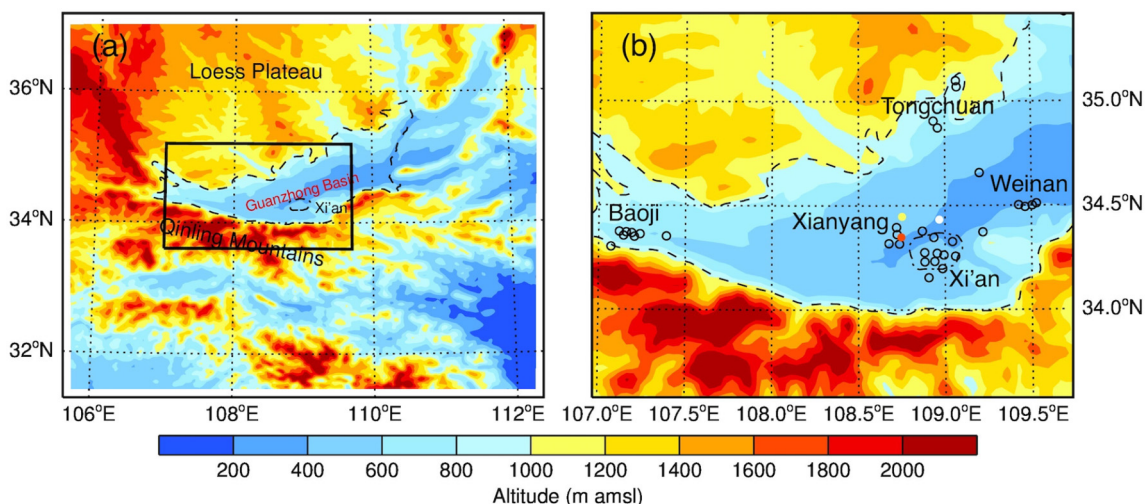


Fig. 1. Maps showing (a) the topography of the study area, and (b) geographic distributions of ambient air quality monitoring stations (black circles) in the five cities in GZB. The white and yellow dots show the locations of the Jinghe and Xianyang weather stations, respectively, and the red dot denotes where the submicron particulate species are measured. The dashed line illustrates the boundary of GZB represented by the 1000 m contour and the dash-dotted line shows the area of Xi'an.

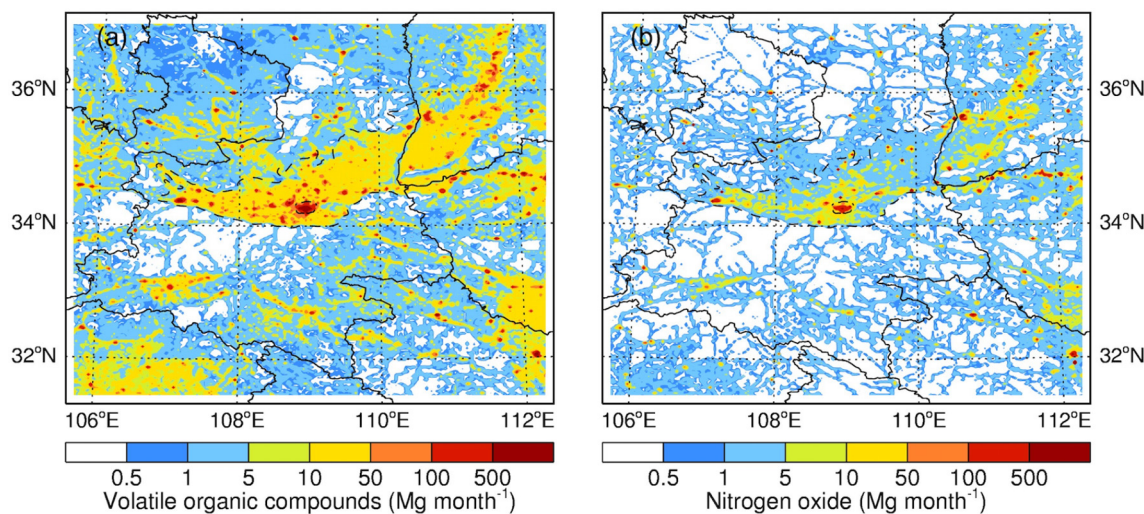


Fig. 2. Geographic distributions of anthropogenic emissions of (a) volatile organic compounds and (b) nitrogen oxide in December 2016 over the simulation domain. The black solid curves present provincial boundaries in China.

WRF-Chem model. [Section 2](#) describes the model and its configurations. [Section 3](#) presents the main body of this study including observation analysis, modeling of the AOC, and investigation of the AOC change on secondary aerosol formation. [Section 4](#) summarizes the main conclusions.

2. Model and method

2.1. Model and configuration

We perform the simulations in this study using a specific version of the WRF-Chem model ([Grell et al., 2005](#)) developed by [Li et al. \(2010, 2011a,b, 2012\)](#). The model adopts a flexible gas-phase chemistry module and the Models-3 community multiscale air quality (CMAQ) aerosol module ([Binkowski and Roselle, 2003](#)). The Fast Tropospheric Ultraviolet and Visible Radiation (FTUV) module is used to calculate the photolysis rates ([Li et al., 2005; Tie et al., 2003](#)), which includes the effects of clouds and aerosols on photochemistry. The gas-phase chemistry module includes a total of 99 chemically interactive species with 330 chemical reactions ([Li et al., 2010, 2011a,b, 2012](#)). The OH formation pathways include O¹D reaction with H₂O, HO₂ reactions with NO and O₃, reactions of unsaturated hydrocarbons with O₃, and the photolysis of HONO, H₂O₂, and OVOCs. The inorganic aerosols are calculated using the ISORROPIA version 1.7 ([Nenes et al., 1998](#)). Besides the SO₂ gas-phase oxidations by OH radical and stabilized creige intermediate (sCI), we also adopt a SO₂ heterogeneous reaction parameterization proposed by [Li et al. \(2017b\)](#). The organic aerosols are simulated using a non-traditional SOA module, which includes the volatility basis-set (VBS) approach ([Donahue et al., 2006; Robinson et al., 2007](#)) and the SOA mass from glyoxal and methylglyoxal ([Volkamer et al., 2007; Zhao et al., 2006](#)). The model takes into account of the aerosol radiative effect in the New Goddard radiation scheme ([Chou and Suarez, 1999](#)). The dry deposition of chemical species is parameterized following [Wesely \(1989\)](#) and the wet deposition is based on the method in the CMAQ module ([Binkowski and Roselle, 2003](#)). The model is configured with grid spacing of 6 km × 6 km (150 × 150 grid cells), which is centered at 38.0°N, 116.0°E ([Fig. 1](#)). The meteorological initial and boundary conditions use the NCEP 1° × 1° reanalysis data and the chemical initial and boundary conditions are interpolated from the Model for OZone And Related chemical Tracers (MOZART) 6 h output ([Horowitz et al., 2003](#)).

An episode from 16 to 21 December 2016 with high O₃ and PM_{2.5} concentrations in GZB is simulated. The adopted anthropogenic emission inventory is from [Zhang et al. \(2009\)](#) and [Li et al. \(2017\)](#), which includes

agriculture, industry, power generation, residential, and transportation sources. [Fig. 2](#) illustrates the spatial distributions of VOCs and NOx emissions over the study area in the inventory during December 2016. The biogenic emissions are predicted by the Model of Emissions of Gases and Aerosol from Nature (MEGAN) model ([Guenther et al., 2006](#)). More information about the model configuration is found in [Table 1](#).

2.2. Calculation of AOC

To assess the AOC quantitatively, [Geyer et al. \(2001\)](#) have proposed a method which treats the AOC as the sum of the respective oxidation rates of the molecules Y_i (VOCs, CO, and CH₄) by the oxidant X (OH, O₃, and NO₃):

$$AOC = \sum k_{Y_i} [Y_i][X] \quad (1)$$

where k_{Y_i} is the rate constant for the reaction of Y_i with X. This calculation considers the concentrations of ambient trace gases and oxidants and also the influence of reaction rates. The air temperature

Table 1
Configurations of the WRF-Chem model.

Item	Configuration
Period	16–21 December 2016
Region	The Guanzhong basin, central China
Domain center	109°E, 34.25°N
Domain size	900 km × 900 km
Horizontal resolution	6 km × 6 km
Vertical resolution	35 vertical levels with a stretched vertical grid with spacing ranging from 50 m near surface, to 500 m at 2.5 km and 1 km above 14 km
Microphysics scheme	WRF Single-Moment 6-class scheme (Hong and Lim, 2006)
Boundary layer scheme	MYJ TKE scheme (Janjić, 2002)
Surface layer scheme	MYJ surface scheme (Janjić, 2002)
Land-surface scheme	Noah land surface model (Chen and Dudhia, 2001)
Longwave radiation scheme	New Goddard scheme (Chou et al., 2001)
Shortwave radiation scheme	New Goddard scheme (Chou and Suarez, 1999)
Meteorological boundary and initial condition	NCEP 1° × 1° reanalysis data
Chemical boundary and initial condition	MOZART 6 h output (Horowitz et al., 2003)
Anthropogenic emission inventory	SAPRC99 chemical mechanism emissions (Zhang et al., 2009; Li et al., 2017)
Biogenic emission inventory	MEGAN model developed by Guenther et al. (2006)
Spin-up time	1 day

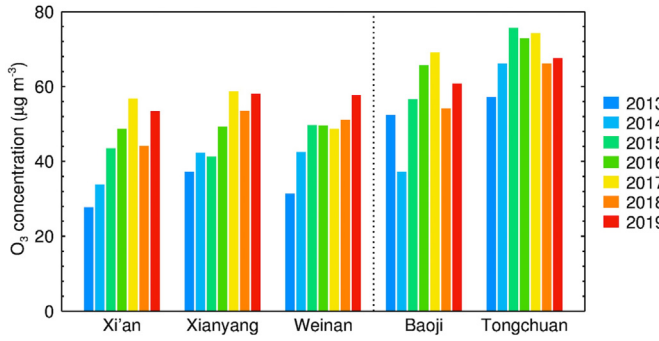


Fig. 3. Histogram showing wintertime (DJF) O_3 concentration in the afternoon (12:00–18:00 LT) during 2013–2019. Note that Xi'an, Xianyang, and Weinan are located in the interior of the basin; Baoji and Tongchuan are situated in the marginal areas (see Fig. 1).

may influence the AOC via the kinetic parameters in the second order reactions (k_{Y_i}). We employ this calculation during the gas phase chemistry iteration in the WRF-Chem model to obtain the AOC over the study domain.

2.3. Pollutant measurements

The pollutant measurements in this study include the hourly O_3 , NO_2 , SO_2 , CO , and $PM_{2.5}$ concentrations at ambient monitoring stations

of China's Ministry of Environment and Ecology (China MEE) which are distributed in the basin (Fig. 1b). These real-time data can be accessed at the website <http://106.37.208.233:20035> and the historical recordings can be retrieved at <http://www.aqistudy.cn>. The hourly contributions of sulfate, nitrate, ammonium, and organic aerosol (OA) in submicron particulate (PM_{1}) are measured by the aerosol chemical speciation monitor (ACSM) in Xianyang (34.35°N, 108.75°E, Fig. 1b) during the study period and the positive matrix factorization (PMF) technique is utilized to identify the secondary fraction of OA.

2.4. Statistics for simulation-measurement comparisons

The statistics including mean bias (MB), root mean square error (RMSE), and index of agreement (IOA) are used to validate the model simulations against measurements (Willmott, 1981):

$$MB = \frac{1}{N} \sum_{i=1}^N (S_i - M_i) \quad (2)$$

$$RMSE = \left[\frac{1}{N} \sum_{i=1}^N (S_i - M_i)^2 \right]^{\frac{1}{2}} \quad (3)$$

$$IOA = 1 - \frac{\sum_{i=1}^N (S_i - M_i)^2}{\sum_{i=1}^N (|S_i - \bar{M}| + |M_i - \bar{M}|)^2} \quad (4)$$

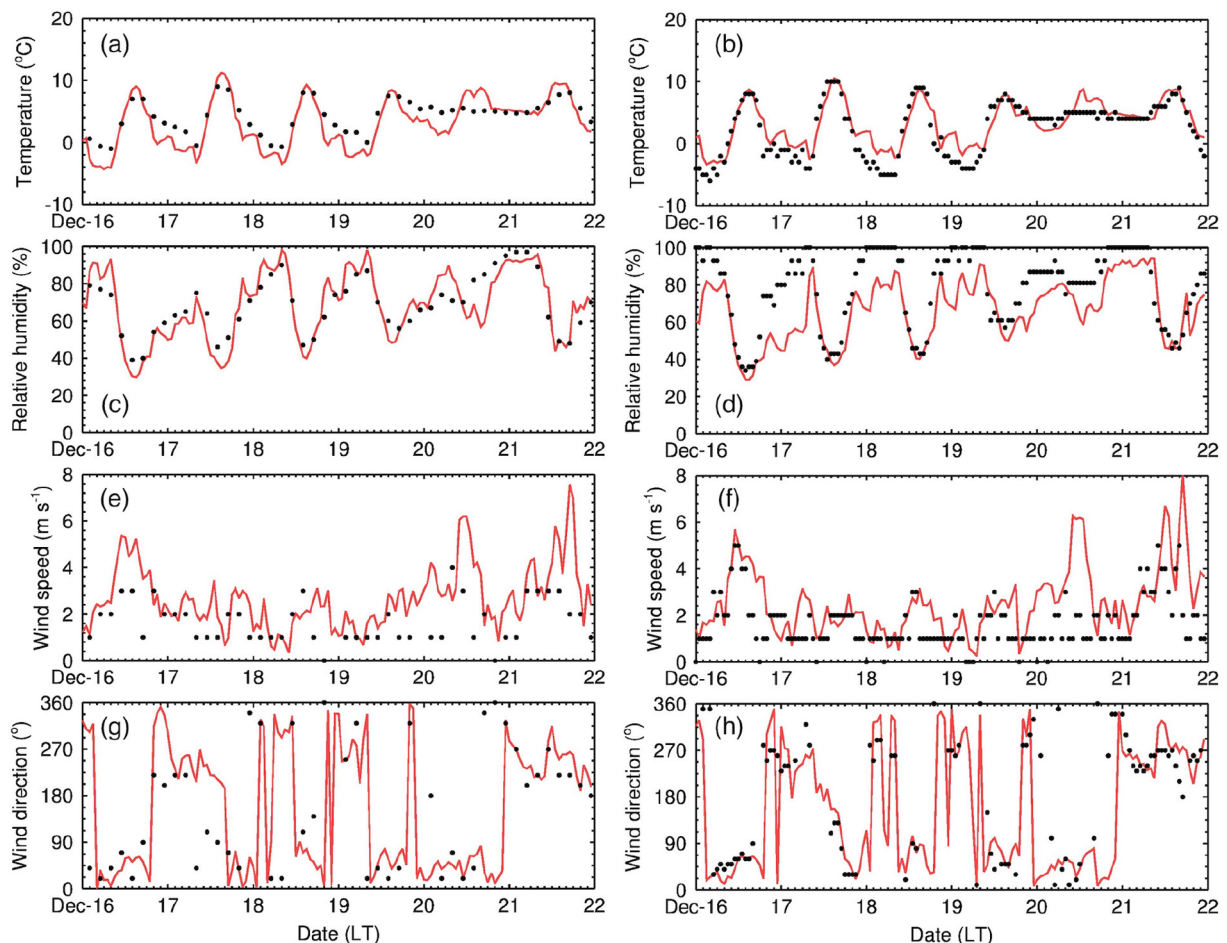


Fig. 4. Temporal variations of the simulated (red curves) and observed (black dots) (a, b) temperature, (c, d) relative humidity, (e, f) wind speed, and (g, h) wind direction at the Jinghe (left panel) and Xianyang (right panel) weather stations from 16 to 21 December 2016.

where S_i and M_i are the simulated and measured variables, respectively. N is the total number of simulated variables and \bar{M} denotes the average of measurements. The IOA ranges from 0 to 1 theoretically, with higher values suggesting better agreement between simulations and measurements.

3. Results and discussion

3.1. Observed ozone increase

The observed wintertime (DJF) O₃ concentration in the afternoon (12:00–18:00 LT) during 2013–2019 in the five cities in GZB is presented in Fig. 3. In Xi'an, Xianyang, and Weinan which are located in the interior of the basin (Fig. 1b), the O₃ concentration has significantly increased by 93%, 56% and 84%, respectively, from 2013 to 2019. In Baoji and Tongchuan, situated in the marginal areas, the O₃ concentration has also considerably increased by 16% and 18%, respectively. These increases suggest that the O₃ levels have elevated remarkably in the vast basin during the past seven years. Since O₃ is one of the key oxidants in the atmosphere, the significant increase in O₃ levels indicates an enhancement of the oxidizing capacity of the atmosphere (Liu et al., 1988), which would exert important impacts on secondary aerosol formation and change the chemical components of airborne particulates.

3.2. Model validation

We define the base simulation in which the emissions from various sources and the atmospheric chemistry are fully included as the reference (REF). The model result in the REF case is compared with the observations to validate the model performance.

3.2.1. Meteorological fields

The meteorological fields play a dominant role in modulating the temporal and spatial evolution of gas-phase and particulate pollutants in the atmosphere (Bei et al., 2016a,b). Fig. 4 presents a comparison for the simulated and observed meteorological parameters including near-surface temperature, relative humidity, wind speed, and wind direction at the Jinghe and Xianyang weather stations which are located in the interior of the basin (Fig. 1b) during the period from 16 to 21 December 2016. Note that the time resolutions for observed meteorological fields at the Jinghe and Xianyang weather stations are 3 h and 1 h, respectively. Observations in Fig. 4a and b show that the near-surface temperature ranges from almost 0 °C to 8 °C at the Jinghe station and from -6 °C to 10 °C at the Xianyang station with clear diurnal cycles during the first three days. Simultaneously, observations at both stations present variable relative humidity ranging from about 40% to 100% (Fig. 4c and d). The model captures the levels and diurnal cycles of the observed temperature and relative humidity very well. The observed wind speed is low during the simulation period, <4 m s⁻¹ and 5 m s⁻¹ at the Jinghe and Xianyang stations, respectively, and lower than 2 m s⁻¹ at most of the time (Fig. 4e and f). The observation shows that the prevailing northeast and southwest winds dominate the wind directions during the study period. The model can well reproduce the low wind profiles at both stations, but slightly overestimates the wind speed occasionally, which is probably due to the simplification of the underlying surface and the inability of the model for microscale simulations (Chen et al., 2011; Lee et al., 2011).

3.2.2. Fine particles and gas-phase species

The hourly measurements including PM_{2.5}, O₃, NO₂, SO₂, and CO concentrations at the ambient monitoring stations (China MEE) in GZB during the study period are utilized to evaluate the model simulation. Fig. 5 presents the temporal variations of the simulated and measured fine particles and gas-phase pollutants averaged over the stations in the basin. The observations show that the PM_{2.5} concentration in the basin increased slowly from about 100 µg m⁻³ on 16 December to

almost 400 µg m⁻³ on 20 December, and then decreased rapidly to 30 µg m⁻³ on 21 December (Fig. 5a). The model well captures the gradual growth of PM_{2.5} concentration from 16 to 19 December and the decline on 21 December, but underestimates the high PM_{2.5} levels on 20 December; the IOA for the PM_{2.5} simulation reaches 0.90. During the study period, the observed O₃ levels (Fig. 5b) are relatively lower compared with other seasons (Feng et al., 2016a,b), but the typical O₃ diurnal cycles with peaks during the afternoon are still clear. The model well reproduces the low O₃ levels and diurnal cycles in the simulation period with an MB of -1.5 µg m⁻³ and an IOA of 0.87, although biases still occur during some peak O₃ time. In terms of the important role of NO₂ in photochemistry and O₃ formation in the troposphere, we compare the simulated and measured NO₂ concentration in the basin. Fig. 5c shows that the simulated NO₂ profile is in good agreement with the measurements, for which the MB is only 0.2 µg m⁻³ and the IOA reaches 0.93. Additionally, the simulated SO₂ and CO concentrations are also compared with the observations in Fig. 5d and e. The model reasonably replicates the SO₂ and CO variations with an IOA of 0.87 and 0.78, respectively, but slightly overestimates the SO₂ level with an MB of 9.9 µg m⁻³.

The spatial distributions of the simulated and observed PM_{2.5} concentration during the study period are further presented in Fig. 6. Both the model simulation and ground-based measurements show a severe particulate pollution event occurred in GZB. On 16 December, the north-east wind prevailed but was blocked by the mountains, and hence local

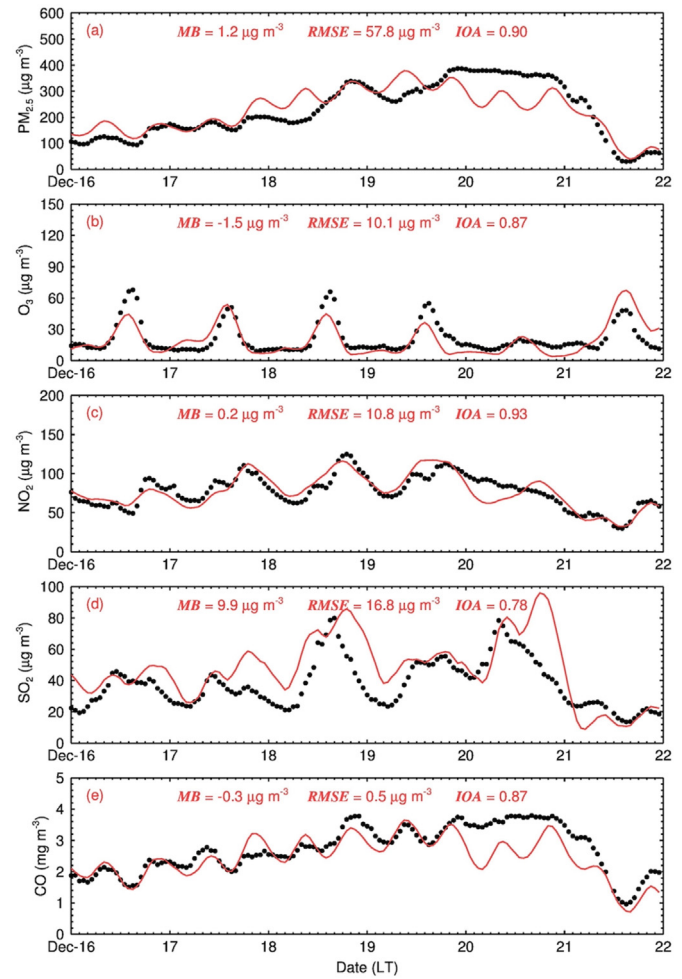


Fig. 5. Temporal variations of the simulated (red curves) and observed (black dots) (a) PM_{2.5}, (b) O₃, (c) NO₂, (d) SO₂, and (e) CO concentrations averaged over the ambient monitoring stations in the basin from 16 to 21 December 2016.

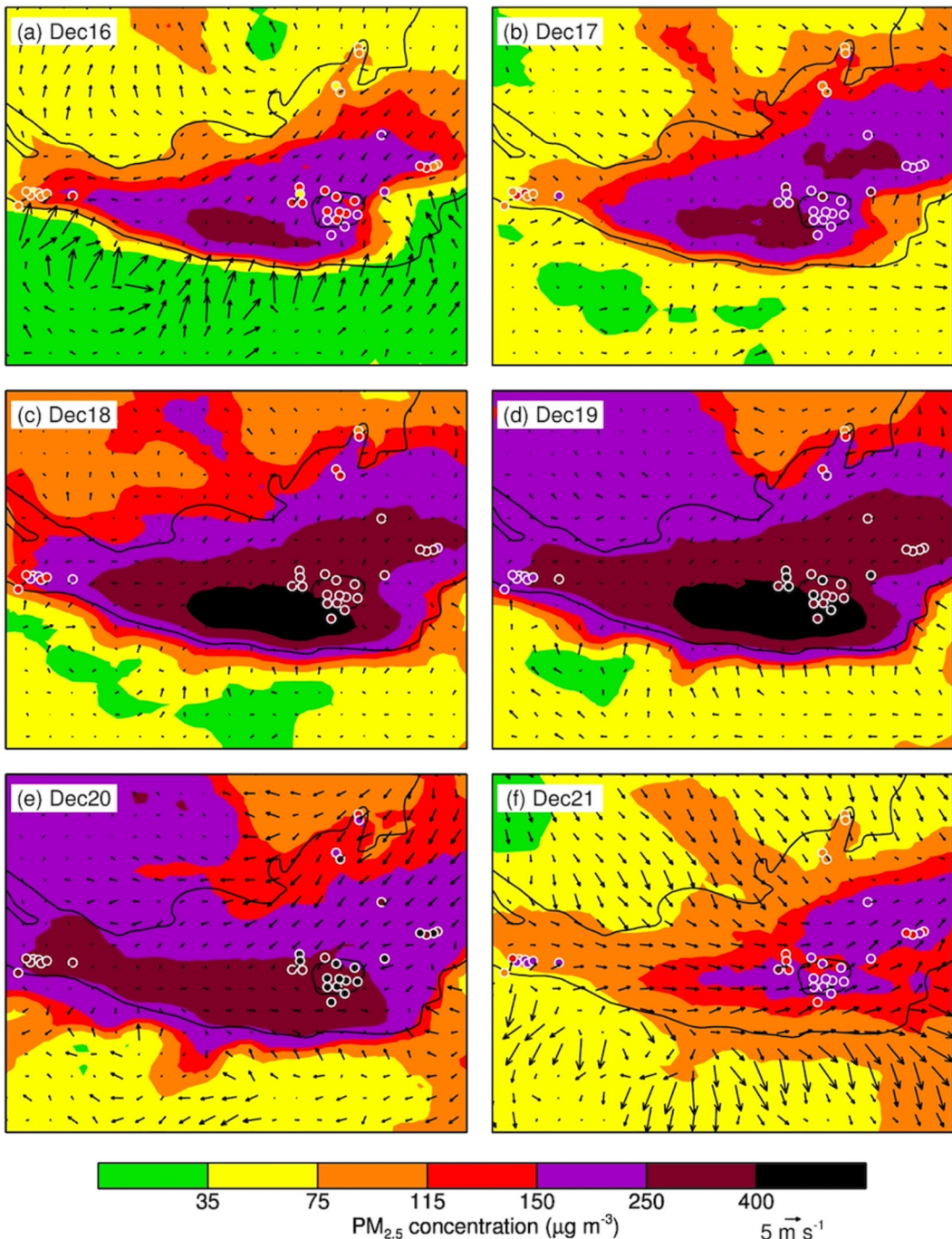


Fig. 6. Spatial distributions of the modeled (colored shadings) and observed (colored dots) daily PM_{2.5} concentration from 16 to 21 December 2016. Arrows show the wind fields.

pollutants started to accumulate. On 17–19 December, the wind in the basin was calm, which is unfavorable for the dispersion of air pollutants and results in severe air pollution in the basin. On 20 December, the northeast wind prevailed again and observations show that the PM_{2.5} concentration at most of the monitoring stations in the basin interior exceeded 400 $\mu\text{g m}^{-3}$. Until 21 December, the west wind took the reins and the airborne particles dispersed quickly. In general, the model simulation well replicates the haze event in the basin, but underestimates the high PM_{2.5} concentration on 20 December as Fig. 5a shows. During this haze event, the evolution of peak O₃ concentration (14:00 LT) in the basin is also presented in Fig. 7. The O₃ concentration was quite low during the haze pollution, particularly in urban areas where the monitoring stations are located in. On 20 December,

the peak O₃ concentration over the entire basin was quite low, indicating that the severe haze pollution suppresses the photochemistry and O₃ formation.

3.2.3. Submicron particle compositions

To further examine the model performance in simulating the aerosol chemical compositions, the simulated sulfate, nitrate, ammonium, total OA, and SOA concentrations in submicron particulate are compared to the hourly observations in Xianyang during the study period (Fig. 8). The observations show that the sulfate, nitrate, and ammonium concentrations increased along with the development of the haze pollution with fluctuations from 16 to 20 December, and then decreased rapidly on 21 December (Fig. 5a). The mean concentrations of observed sulfate,

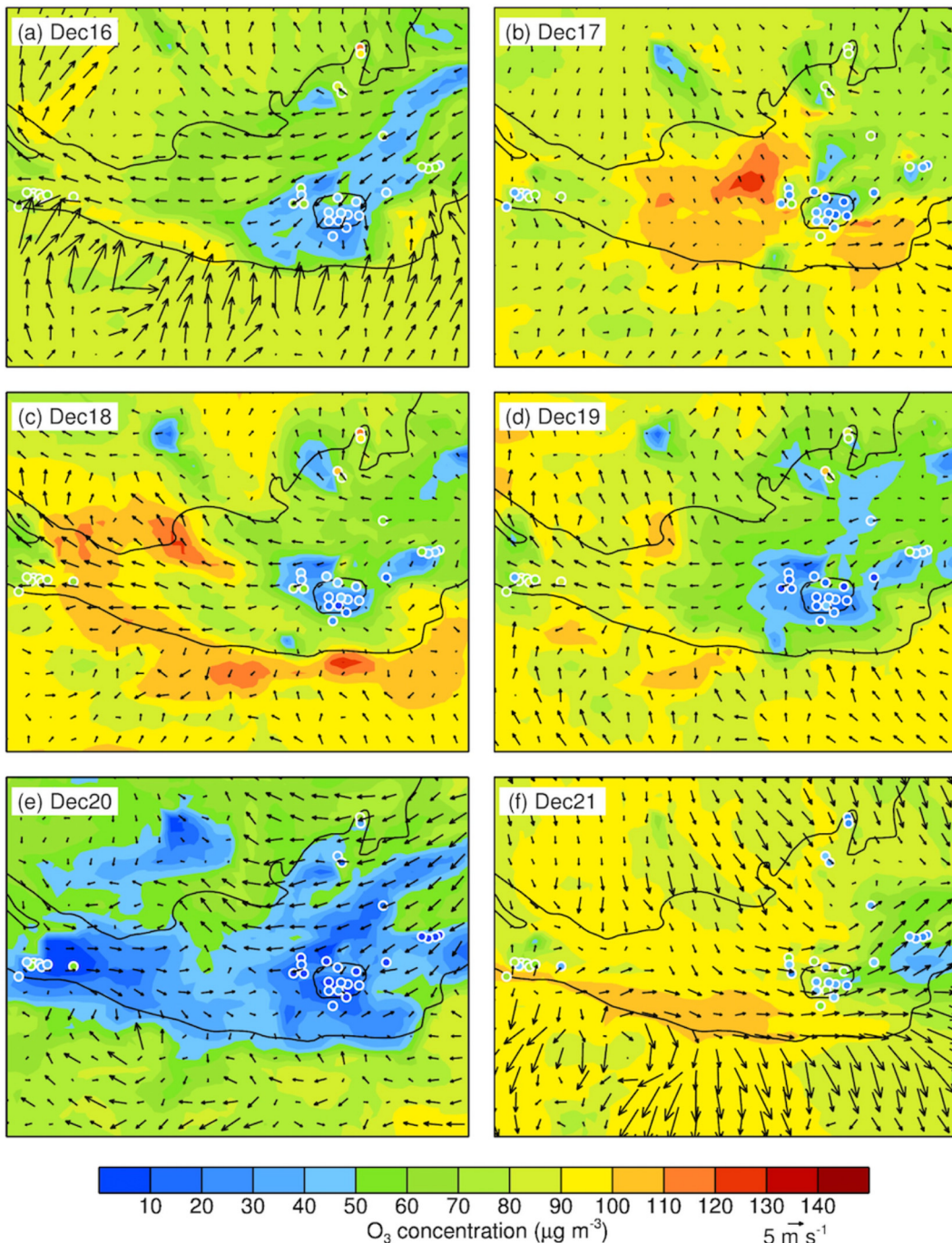


Fig. 7. Spatial distributions of the modeled (colored shadings) and observed (colored dots) O_3 concentration at 14:00 LT from 16 to 21 December 2016. Arrows show the wind fields.

nitrate, and ammonium aerosols in submicron particles are $17.8 \mu\text{g m}^{-3}$, $24.3 \mu\text{g m}^{-3}$, and $16.9 \mu\text{g m}^{-3}$, respectively. The model is able to reproduce the gradual increases and rapid declines with IOAs of 0.77, 0.79, and 0.80 for sulfate, nitrate, and ammonium aerosols. OA, with a mean concentration of $60.5 \mu\text{g m}^{-3}$ during the study period, constitutes the most important contributor for the submicron particle mass, and about 39% of the OA mass is attributed to the secondary fraction. The model reasonably replicates the OA and SOA levels during the haze event with IOAs of 0.71 and 0.79, respectively. Overall, the model performs reasonably well in simulating the submicron aerosols, but discrepancies still exist and are even remarkable at times. The model biases are largely attributed to the

uncertainty in the simulated meteorological field and emission inventory, since Xianyang is located in the northwest adjacent area of Xi'an, the biggest city in GZB with a large amount of emissions (Fig. 2).

3.3. Correlations between AOC and O_3/NO_2 concentrations

The calculation of AOC is complicated in the model, which involves hundreds of chemical reactions in the atmosphere. It would be convenient to assess the AOC levels if any AOC indicators are available. Hourly O_3 and NO_2 concentrations, closely associated with the AOC, are measured at the ambient monitoring stations

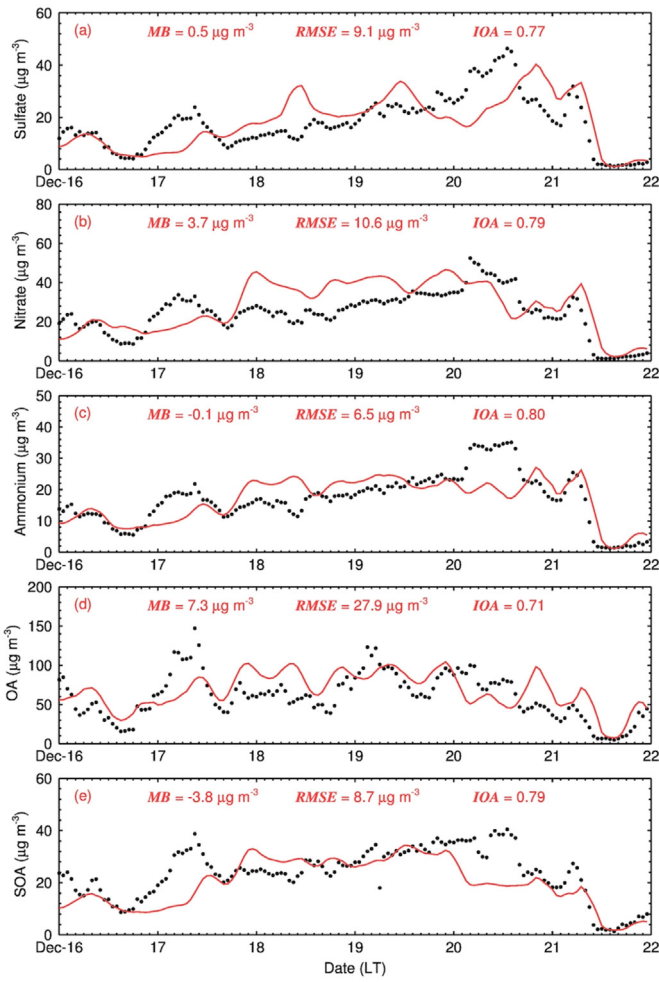


Fig. 8. Temporal variations of the simulated (red curves) and observed (black dots) (a) sulfate, (b) nitrate, (c) ammonium, (d) OA, and (e) SOA concentrations in Xianyang from 16 to 21 December 2016.

(China MEE). If these species are good AOC indicators, it would be much easier to access the AOC level.

We analyze the relationships between the AOC and O_3/NO_2 concentrations in the basin. Fig. 9a–c present scatter plots for the hourly AOC versus O_3 , NO_2 , and $O_x (=O_3 + NO_2)$ concentrations during the study period. Among these plots, the population O_x concentration is significantly correlated with the AOC ($r = 0.58, p < 0.01$), suggesting that the population O_x concentration can serve as a good AOC tracer. Although both the population O_3 and NO_2 concentrations are also correlated with the hourly AOC, the correlation coefficients are lower ($r = 0.54, p < 0.01$ and $r = 0.21, p < 0.05$, respectively). When the time is confined to the afternoon (12:00–18:00 LT), the positive correlation between the AOC and O_x concentration is much more significant for afternoon average ($r = 0.92, p < 0.01$, Fig. 9g–i). A positive correlation between the AOC and NO_2 concentration also exists, but less remarkable ($r = 0.83, p < 0.01$), and the correlation between the AOC and O_3 concentration is not significant. Therefore, we propose that both the population hourly and postmeridian O_x concentration can be used as tracers for the wintertime AOC in the basin.

3.4. Sensitivity experiments

Five sensitivity experiments are performed to explore the impacts of AOC changes on airborne particulates and particularly on the secondary fractions. Since the AOC is mainly resulted from the photochemical

reactions in the atmosphere, we reduce the photolysis rates for the photochemical reactions by various levels to attenuate the AOC artificially. In the sensitivity experiments SEN1–5, the photolysis rates are reduced to 50% at an interval of 10%. Results from the sensitivity simulations are compared to the REF case to examine the influence of AOC changes upon aerosol compositions.

3.4.1. AOC and O_x changes

The diurnal profiles of AOC and O_x concentration within the basin in SEN1–5 are compared with the REF simulation to present the AOC changes in the five sensitivity experiments. Fig. 10a shows that the AOC in the sensitivity simulations remarkably decreases during daytime and to extremely low levels during nighttime hours. The O_x concentration varies following the fluctuations of the AOC with a lag of 2 h (Fig. 10b). The O_x concentration reaches its maximum in the afternoon and the nighttime concentration is still high, which is attributed to the high NO_2 levels due to the titration of NO with O_3 (Feng et al., 2016a). In the five sensitivity experiments, the daytime AOC decreases significantly, particularly during the noon hours (Fig. 10a); for the SEN5 experiment, the AOC decreases by about 38% compared with the REF simulation. Similarly, the O_x concentration also decreases remarkably in the five sensitivity experiments, especially in the afternoon, and the mean O_x concentration in the SEN5 case is around 13% lower than that in the REF simulation.

3.4.2. $PM_{2.5}$ concentration changes

The impacts of the AOC changes on $PM_{2.5}$ concentration are analyzed through a comparison between the sensitivity experiments and the REF simulation. Fig. 11 shows that compared with the REF simulation, the $PM_{2.5}$ concentration averaged over the simulation period decreases almost linearly from $227.0 \mu g m^{-3}$ to $209.1 \mu g m^{-3}$ as the AOC is attenuated from $24.15 \times 10^6 cm^{-3} s^{-1}$ to $14.95 \times 10^6 cm^{-3} s^{-1}$ in the basin; the slope for the changes in $PM_{2.5}$ concentration and AOC is about $1.94 (\mu g m^{-3})/(10^6 cm^{-3} s^{-1})$. Fig. 12 presents the temporal profiles of changes in $PM_{2.5}$ concentration in the sensitivity experiments compared with the REF simulation in the basin. The AOC changes exert considerable influences on the $PM_{2.5}$ concentration, particularly during the episodes with high $PM_{2.5}$ concentration (Fig. 5). In the five sensitivity experiments, the $PM_{2.5}$ concentration averaged over the simulation period decreases by 1.4%, 2.9%, 4.5%, 6.1%, and 7.9%, respectively, as the average AOC decreases by 7.3%, 14.6%, 22.2%, 29.8%, and 38.1%. In the SEN5 case with the AOC reduced most remarkably, the $PM_{2.5}$ concentration decreases by $>30 \mu g m^{-3}$ ($>10\%$) during peak time.

3.4.3. Secondary aerosol changes

The secondary aerosols in $PM_{2.5}$ are formed through chemical reactions participated by oxidants such as OH , O_3 , and NO_3 in the atmosphere which are the main contributors to the AOC. In general, the impacts of AOC on secondary aerosol formation can be represented using the following oxidation processes in the atmosphere:



The gas phase reactions for sulfate formation include the oxidation of $S(IV)$ by OH , H_2O_2 , O_3 (Seinfeld and Pandis, 2006; Stein and Saylor, 2012), and stabilized creige intermediate (SCI) (Li et al., 2013; L. Liu et al., 2019; Sarwar et al., 2014; Ying et al., 2014). Note that the heterogeneous reactions on aerosol surface for sulfate and nitrate formation are generally not considered in terms of the AOC. Since ammonium

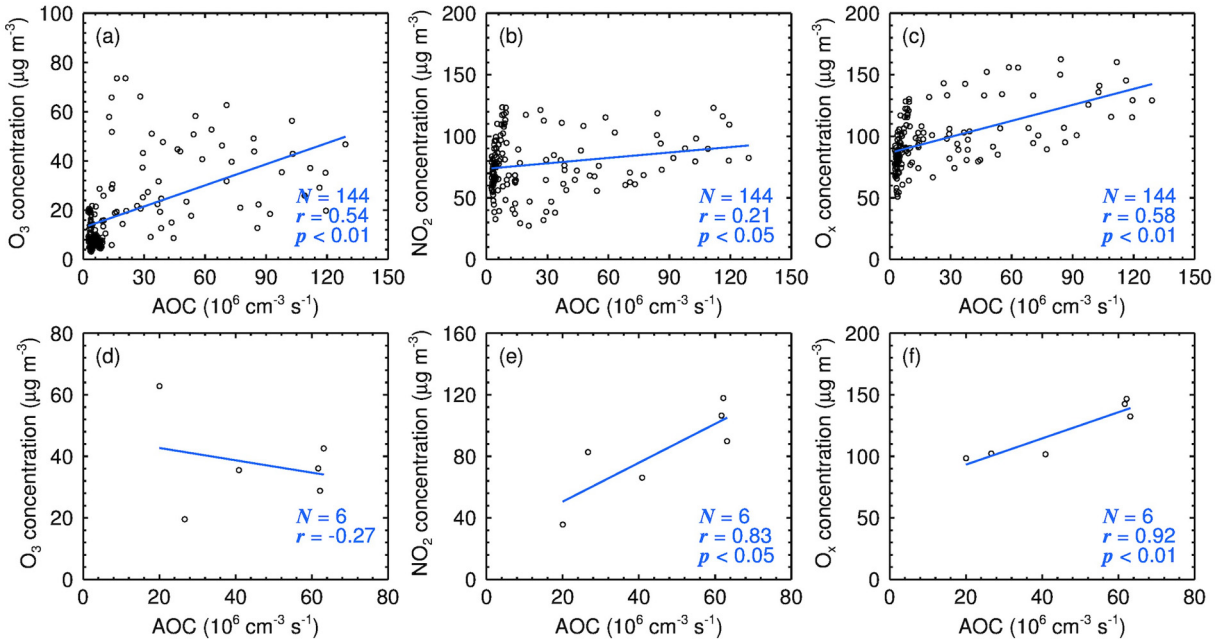


Fig. 9. Scatter plots showing the correlations between the AOC and O_3 (NO_2 , O_x) concentration in the basin during the period from 16 to 21 December 2016. The upper panels denote the correlations for hourly data all day long; the middle panels are for the correlations for hourly data in the afternoon (12:00–18:00 LT); the lower panels are for the correlations for averaged data in the afternoon (12:00–18:00 LT).

usually acts as the main base material neutralizing the acid sulfate and nitrate, it is also treated as secondary aerosol in the atmosphere. The last three reactions are for the SOA formation, which includes the oxidation and partitioning of VOCs, IVOCs, and primary organic gases (POGs) from evaporation of semi-volatile primary organic aerosol.

Fig. 11 presents the impacts of AOC changes on sulfate, nitrate, ammonium, and SOA concentrations in the basin averaged over the study period. Following the attenuation of AOC in the sensitivity experiments, the concentrations of all the four secondary aerosols decrease approximately linearly. The sensitivity experiments propose that the AOC change exerts the most significant impact on the SOA formation with a slope of $0.83 (\mu\text{g m}^{-3})/(10^6 \text{ cm}^{-3} \text{ s}^{-1})$ for $\Delta(\text{SOA})/\Delta(\text{AOC})$, followed by the nitrate formation with a slope of $0.78 (\mu\text{g m}^{-3})/(10^6 \text{ cm}^{-3} \text{ s}^{-1})$. As a comparison, the influences on

sulfate and ammonium concentrations are much less, i.e. $0.11 (\mu\text{g m}^{-3})/(10^6 \text{ cm}^{-3} \text{ s}^{-1})$ and $0.21 (\mu\text{g m}^{-3})/(10^6 \text{ cm}^{-3} \text{ s}^{-1})$, respectively. Fig. 13 further shows the diurnal profiles of the secondary aerosol concentrations in the sensitivity experiments differentiating the REF simulation. Remarkable decreases in the nitrate and SOA concentrations are presented as the AOC decreases in the study period, especially during the severely polluted episodes (Fig. 5a). In the SEN5 experiment, the nitrate and SOA concentrations decrease by $>15 \mu\text{g m}^{-3}$ during peak time, and the ammonium aerosol decreases by $>4 \mu\text{g m}^{-3}$. The decrease in sulfate concentration is quite minor during the entire period ($<2 \mu\text{g m}^{-3}$), which is likely because sulfate aerosol is mainly formed in the heterogeneous processes on aerosol surface (Li et al., 2017a). This result suggests that the change in AOC can greatly affect the formation of secondary aerosols and hence the total $\text{PM}_{2.5}$ concentration. Meanwhile, the responses of

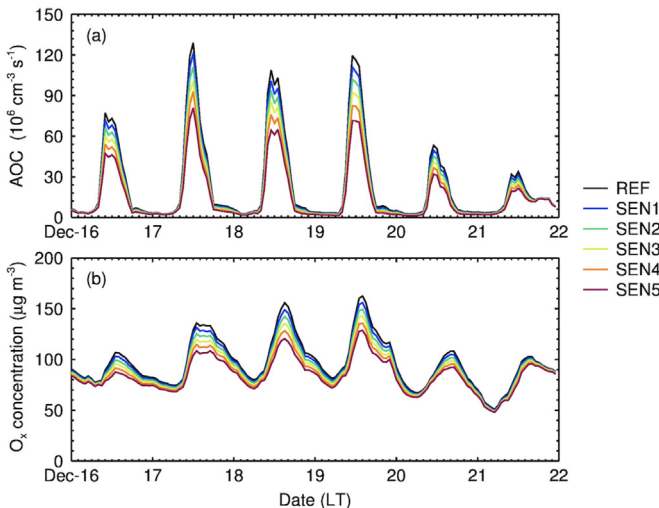


Fig. 10. Temporal variations of the simulated (a) AOC and (b) O_x concentration in the base simulation and sensitivity experiments in GZB from 16 to 21 December 2016.

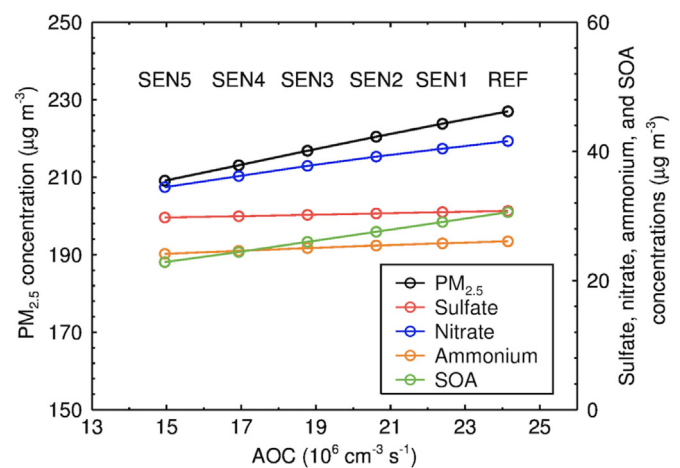


Fig. 11. Relationships between the AOC levels and the $\text{PM}_{2.5}$, sulfate, nitrate, ammonium, and SOA concentrations averaged over the simulation period in the basin from the REF simulation and sensitivity experiments.

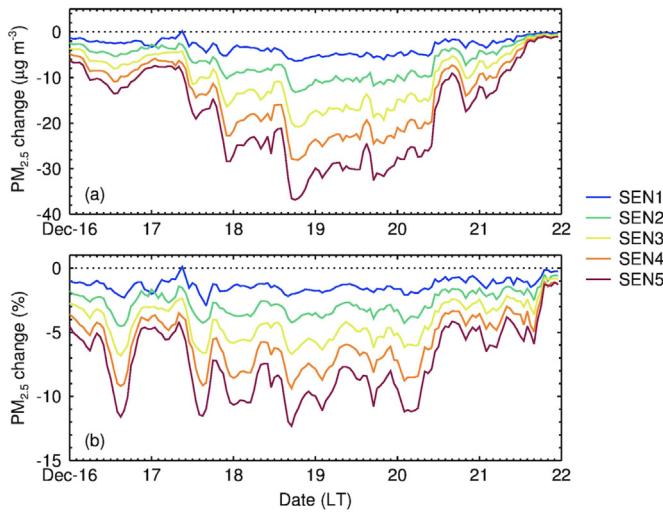


Fig. 12. Temporal variations of PM_{2.5} (a) concentration and (b) percentage changes in the sensitivity experiments compared to the base simulation (SENi – REF) in GZB from 16 to 21 December 2016.

secondary aerosol components to the AOC change are different; nitrate and SOA aerosols are sensitive to the AOC change, but sulfate is less sensitive.

4. Summary and implications

During recent years, the observed near-surface O₃ concentration in GZB has increased significantly in winter, indicating a remarkable enhancement of the AOC. Since the secondary aerosols in airborne particles are formed during the oxidation processes in the atmosphere, the enhancement of the AOC potentially facilitates the formation of secondary aerosols. In this study, we assess the impact of the recent AOC enhancement on the PM_{2.5} concentration and the formation of the main secondary components including sulfate, nitrate, ammonium, and SOA during wintertime in GZB using the WRF-Chem model.

The model simulation well replicates the meteorological fields observed at the Jinghe and Xianyang weather stations in the interior of the basin. The predicted temporal variations of PM_{2.5} concentration

and gas-phase species including O₃, NO₂, SO₂, and CO are in good agreement with the measurements averaged over the monitoring stations distributed in the basin (an IOA of 0.78–0.93). Spatially, the model performs reasonably in simulating the high PM_{2.5} but low O₃ levels over the interior area of the basin during the severe haze episode from 18 to 20 December 2016. In general, the model simulation can reproduce the observed temporal profiles of submicron particulate compositions including sulfate, nitrate, ammonium, total OA, and SOA in Xianyang with an IOA of 0.71–0.80, although discrepancies between the model and measurements still exist.

The relationships between the AOC and O_x concentration in the basin during the simulation period are analyzed, which presents good positive correlations between the population hourly AOC and O_x concentration as well as the population AOC and O_x concentration averaged over the afternoon (12:00–18:00 LT). This result proposes that the population hourly and postmeridian O_x concentration have a potential to be used as simplified indicators for the wintertime AOC in the basin.

Sensitivity experiments are devised to examine the influences of the AOC changes on ambient particulates, especially on the formation of secondary aerosols. Following the AOC, the O_x concentration in the sensitivity simulations decreases as the total AOC is attenuated, but with a lag of about 2 h for the peak time. The AOC decreases in the sensitivity experiments almost result in a linear reduction in total PM_{2.5} concentration in the basin with a rate of $1.94 (\mu\text{g m}^{-3})/(10^6 \text{ cm}^{-3} \text{ s}^{-1})$. This reduction is attributed to the decreases in the secondary fractions in PM_{2.5}, i.e. $0.83 (\mu\text{g m}^{-3})/(10^6 \text{ cm}^{-3} \text{ s}^{-1})$ for SOA, $0.78 (\mu\text{g m}^{-3})/(10^6 \text{ cm}^{-3} \text{ s}^{-1})$ for nitrate aerosol, $0.21 (\mu\text{g m}^{-3})/(10^6 \text{ cm}^{-3} \text{ s}^{-1})$ for ammonium aerosol, and $0.11 (\mu\text{g m}^{-3})/(10^6 \text{ cm}^{-3} \text{ s}^{-1})$ for the sulfate component. The large difference in the responses of secondary aerosols to the AOC changes is associated with their different formation pathways in the air. The oxidation of gas-phase precursors plays important roles in the formation of nitrate aerosol and SOA, while the sulfate aerosol is mainly formed from the heterogeneous processes (Li et al., 2017a).

Credit author statement

TF and SZ designed research; TF performed model simulation and wrote paper; QW performed submicron particle measurement; XZ and LL analyzed data; GL and XT revised paper.

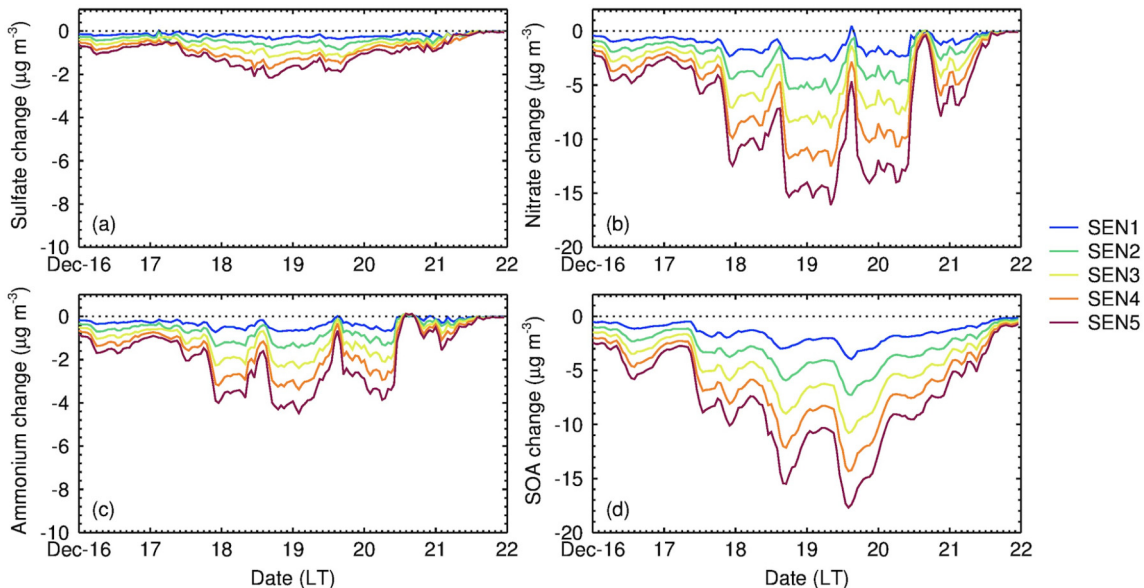


Fig. 13. Temporal variations of changes in (a) sulfate, (b) nitrate, (c) ammonium, and (d) SOA in PM_{2.5} in the sensitivity experiments compared to the base simulation (SENi – REF) in GZB from 16 to 21 December 2016.

Declaration of competing interest

The authors declare that they have no conflict of interest.

Acknowledgements

This work was supported by the National Natural Science Foundation of China (no. 41703127) and the Natural Science Foundation of Zhejiang Province (no. LZ20D050001). This study was also sponsored by K. C. Wong Magna Fund in Ningbo University.

References

- Bei, N., Li, G., Huang, R.-J., Cao, J., Meng, N., Feng, T., Liu, S., Zhang, T., Zhang, Q., Molina, L.T., 2016a. Typical synoptic situations and their impacts on the wintertime air pollution in the Guanzhong basin, China. *Atmos. Chem. Phys.* 16, 7373–7387. <https://doi.org/10.5194/acp-16-7373-2016>.
- Bei, N., Xiao, B., Meng, N., Feng, T., 2016b. Critical role of meteorological conditions in a persistent haze episode in the Guanzhong basin, China. *Sci. Total Environ.* 550, 273–284. <https://doi.org/10.1016/j.scitotenv.2015.12.159>.
- Binkowski, F.S., Roselle, S.J., 2003. Models-3 Community Multiscale Air Quality (CMAQ) model aerosol component 1. Model description. *J. Geophys. Res.* 108, 4183. <https://doi.org/10.1029/2001JD001409>.
- Cao, J., Wang, Q.Y., Chow, J.C., Watson, J.G., Tie, X.X., Shen, Z.X., Wang, P., An, Z.S., 2012a. Impacts of aerosol compositions on visibility impairment in Xi'an, China. *Atmos. Environ.* 59, 559–566. <https://doi.org/10.1016/j.atmosenv.2012.05.036>.
- Cao, J., Xu, H., Xu, Q., Chen, B., Kan, H., 2012b. Fine particulate matter constituents and cardiopulmonary mortality in a heavily polluted Chinese city. *Environ. Health Perspect.* 120, 373–378. <https://doi.org/10.1289/ehp.1103671>.
- Chen, F., Dudhia, J., 2001. Coupling an advanced land surface-hydrology model with the Penn State-NCAR MM5 modeling system. Part II: preliminary model validation. *Mon. Weather Rev.* 129, 569–585. [https://doi.org/10.1175/1520-0493\(2001\)129<0569:caalsh>2.0.co;2](https://doi.org/10.1175/1520-0493(2001)129<0569:caalsh>2.0.co;2).
- Chen, F., Kusaka, H., Bornstein, R., Ching, J., Grimmond, C.S.B., Grossman-Clarke, S., Loridan, T., Manning, K.W., Martilli, A., Miao, S., Sailor, D., Salamanca, F.P., Taha, H., Tewari, M., Wang, X., Wyszogrodzki, A.A., Zhang, C., 2011. The integrated WRF/urban modelling system: development, evaluation, and applications to urban environmental problems. *Int. J. Climatol.* 31, 273–288. <https://doi.org/10.1002/joc.2158>.
- Cheng, N., Li, Y., Zhang, D., Chen, T., Sun, F., Chen, C., Meng, F., 2016. Characteristics of ground ozone concentration over Beijing from 2004 to 2015: trends, transport, and effects of reductions. *Atmos. Chem. Phys. Discuss.*, 1–21 <https://doi.org/10.5194/acp-2016-508>.
- Chou, M.-D., Suarez, M.J., 1999. A solar radiation parameterization for atmospheric studies (no. NASA/TM-1999-10460). NASA Technique Report.
- Chou, M.-D., Suarez, M.J., Liang, X.-Z., Yan, M.M.H., 2001. A thermal infrared radiation parameterization for atmospheric studies (no. NASA/TM-2001-104606). NASA Technique Report.
- Donahue, N.M., Robinson, A.L., Staniar, C.O., Pandis, S.N., 2006. Coupled partitioning, dilution, and chemical aging of semivolatile organics. *Environ. Sci. Technol.* 40, 2635–2643. <https://doi.org/10.1021/es052297c>.
- Elshorbagy, Y.F., Kurtenbach, R., Wiesen, P., Lissi, E., Rubio, M., Villena, G., Gramsch, E., Rickard, A.R., Pilling, M.J., Kleffmann, J., 2009. Oxidation capacity of the city air of Santiago, Chile. *Atmos. Chem. Phys.* 9, 2257–2273. <https://doi.org/10.5194/acp-9-2257-2009>.
- Feng, T., Bei, N., Huang, R.-J., Cao, J., Zhang, Q., Zhou, W., Tie, X., Liu, S., Zhang, T., Su, X., Lei, W., Molina, L.T., Li, G., 2016a. Summertime ozone formation in Xi'an and surrounding areas, China. *Atmos. Chem. Phys.* 16, 4323–4342. <https://doi.org/10.5194/acp-16-4323-2016>.
- Feng, T., Li, G., Cao, J., Bei, N., Shen, Z., Zhou, W., Liu, S., Zhang, T., Wang, Y., Huang, R.-J., Tie, X., Molina, L.T., 2016b. Simulations of organic aerosol concentrations during springtime in the Guanzhong Basin, China. *Atmos. Chem. Phys.* 16, 10045–10061. <https://doi.org/10.5194/acp-16-10045-2016>.
- Feng, T., Bei, N., Zhao, S., Wu, J., Li, X., Zhang, T., Cao, J., Zhou, W., Li, G., 2018. Wintertime nitrate formation during haze days in the Guanzhong basin, China: a case study. *Environ. Pollut.* 243, 1057–1067. <https://doi.org/10.1016/j.envpol.2018.09.069>.
- Feng, T., Zhao, S., Bei, N., Wu, J., Liu, S., Li, X., Liu, L., Qian, Y., Yang, Q., Wang, Y., Zhou, W., Cao, J., Li, G., 2019. Secondary organic aerosol enhanced by increasing atmospheric oxidizing capacity in Beijing-Tianjin-Hebei (BTH), China. *Atmos. Chem. Phys.* 19, 7429–7443. <https://doi.org/10.5194/acp-19-7429-2019>.
- Fuchs, H., Tan, Z., Lu, K., Bohn, B., Broch, S., Brown, S.S., Dong, H., Gomm, S., Häseler, R., He, L., Hofzumahaus, A., Holland, F., Li, X., Liu, Y., Lu, S., Min, K.-E., Rohrer, F., Shao, M., Wang, B., Wang, M., Wu, Y., Zeng, L., Zhang, Y., Wahner, A., Zhang, Y., 2017. OH reactivity at a rural site (Wangdu) in the North China Plain: contributions from OH reactants and experimental OH budget. *Atmos. Chem. Phys.* 17, 645–661. <https://doi.org/10.5194/acp-17-645-2017>.
- Gao, W., Tie, X., Xu, J., Huang, R., Mao, X., Zhou, G., Chang, L., 2017. Long-term trend of O₃ in a mega City (Shanghai), China: characteristics, causes, and interactions with precursors. *Sci. Total Environ.* 603–604, 425–433. <https://doi.org/10.1016/j.scitotenv.2017.06.099>.
- Geyer, A., Aliche, B., Konrad, S., Schmitz, T., Stutz, J., Platt, U., 2001. Chemistry and oxidation capacity of the nitrate radical in the continental boundary layer near Berlin. *J. Geophys. Res.* 106, 8013–8025. <https://doi.org/10.1029/2000JD900681>.
- Grell, G.A., Peckham, S.E., Schmitz, R., McKeen, S.A., Frost, G., Skamarock, W.C., Eder, B., 2005. Fully coupled “online” chemistry within the WRF model. *Atmos. Environ.* 39, 6957–6975. <https://doi.org/10.1016/j.atmosenv.2005.04.027>.
- Guenther, A., Karl, T., Harley, P., Wiedinmyer, C., Palmer, P.J., Geron, C., 2006. Estimates of global terrestrial isoprene emissions using MEGAN (Model of Emissions of Gases and Aerosols from Nature). *Atmos. Chem. Phys.* 6, 3181–3210. <https://doi.org/10.5194/acp-6-3181-2006>.
- Hong, S.Y., Lim, J., 2006. The WRF single-moment 6-class microphysics scheme (WSM6). *Asia-Pac. J. Atmos. Sci.* 42, 129–151.
- Horowitz, L.W., Walters, S., Mauzerall, D.L., Emmons, L.K., Rasch, P.J., Granier, C., Tie, X., Lamarque, J.-F., Schultz, M.G., Tyndall, G.S., Orlando, J.J., Brasseur, G.P., 2003. A global simulation of tropospheric ozone and related tracers: description and evaluation of MOZART, version 2. *J. Geophys. Res.* 108, 4784. <https://doi.org/10.1029/2002jd002853>.
- Janjić, Z.I., 2002. Nonsingular Implementation of the Mellor-Yamada Level 2.5 Scheme in the NCEP Meso Model (No. 437). NCEP Office Note.
- Kim, Y.J., Spak, S.N., Carmichael, G.R., Riemer, N., Stanier, C.O., 2014. Modeled aerosol nitrate formation pathways during wintertime in the Great Lakes region of North America. *J. Geophys. Res.* 119, 12,420–12,445. <https://doi.org/10.1002/2014JD022320>.
- Lee, S.H., Kim, S.W., Angevine, W.M., Bianco, L., McKeen, S.A., Senff, C.J., Trainer, M., Tucker, S.C., Zamora, R.J., 2011. Evaluation of urban surface parameterizations in the WRF model using measurements during the Texas Air Quality Study 2006 field campaign. *Atmos. Chem. Phys.* 11, 2127–2143. <https://doi.org/10.5194/acp-11-2127-2011>.
- Lelieveld, J., Gromov, S., Pozzer, A., Taraborrelli, D., 2016. Global tropospheric hydroxyl distribution, budget and reactivity. *Atmos. Chem. Phys.* 16, 12477–12493. <https://doi.org/10.5194/acp-16-12477-2016>.
- Li, G., Zhang, R., Fan, J., Tie, X., 2005. Impacts of black carbon aerosol on photolysis and ozone. *J. Geophys. Res.* 110, D23206. <https://doi.org/10.1029/2005JD005898>.
- Li, G., Wang, Y., Zhang, R., 2008. Implementation of a two-moment bulk microphysics scheme to the WRF model to investigate aerosol-cloud interaction. *J. Geophys. Res.* 113, D15211. <https://doi.org/10.1029/2007JD009361>.
- Li, G., Wang, Y., Lee, K.-H., Diao, Y., Zhang, R., 2009. Impacts of aerosols on the development and precipitation of a mesoscale squall line. *J. Geophys. Res.* 114, D17205. <https://doi.org/10.1029/2008JD011581>.
- Li, G., Lei, W., Zavala, M., Volkamer, R., Dusanter, S., Stevens, P., Molina, L.T., 2010. Impacts of HONO sources on the photochemistry in Mexico City during the MCMA-2006/MILAGRO Campaign. *Atmos. Chem. Phys.* 10, 6551–6567. <https://doi.org/10.5194/acp-10-6551-2010>.
- Li, G., Bei, N., Tie, X., Molina, L.T., 2011a. Aerosol effects on the photochemistry in Mexico City during MCMA-2006/MILAGRO campaign. *Atmos. Chem. Phys.* 11, 5169–5182. <https://doi.org/10.5194/acp-11-5169-2011>.
- Li, G., Zavala, M., Lei, W., Tsimplidi, A.P., Karydis, V.A., Pandis, S.N., Canagaratna, M.R., Molina, L.T., 2011b. Simulations of organic aerosol concentrations in Mexico City using the WRF-CHEM model during the MCMA-2006/MILAGRO campaign. *Atmos. Chem. Phys.* 11, 3789–3809. <https://doi.org/10.5194/acp-11-3789-2011>.
- Li, G., Lei, W., Bei, N., Molina, L.T., 2012. Contribution of garbage burning to chloride and PM_{2.5} in Mexico City. *Atmos. Chem. Phys.* 12, 8751–8761. <https://doi.org/10.5194/acp-12-8751-2012>.
- Li, J., Ying, Q., Yi, B., Yang, P., 2013. Role of stabilized Criegee Intermediates in the formation of atmospheric sulfate in eastern United States. *Atmos. Environ.* 79, 442–447. <https://doi.org/10.1016/j.atmosenv.2013.06.048>.
- Li, M., Zhang, Q., Kurokawa, J.-I., Woo, J.-H., He, K., Lu, Z., Ohara, T., Song, Y., Streets, D.G., Carmichael, G.R., Cheng, Y., Hong, C., Huo, H., Jiang, X., Kang, S., Liu, F., Su, H., Zheng, B., 2017. MIX: a mosaic Asian anthropogenic emission inventory under the international collaboration framework of the MICS-Asia and HTAP. *Atmos. Chem. Phys.* 17, 935–963. <https://doi.org/10.5194/acp-17-935-2017>.
- Li, G., Bei, N., Cao, J., Huang, R., Wu, J., Feng, T., Wang, Y., Liu, S., Zhang, Q., Tie, X., Molina, L.T., 2017a. A possible pathway for rapid growth of sulfate during haze days in China. *Atmos. Chem. Phys.* 17, 3301–3316. <https://doi.org/10.5194/acp-17-3301-2017>.
- Li, G., Bei, N., Cao, J., Wu, J., Long, X., Feng, T., Dai, W., Liu, S., Zhang, Q., Tie, X., 2017b. Widespread and persistent ozone pollution in eastern China during the non-winter season of 2015: observations and source attributions. *Atmos. Chem. Phys.* 17, 2759–2774. <https://doi.org/10.5194/acp-17-2759-2017>.
- Li, N., He, Q., Greenberg, J., Guenther, A., Li, J., Cao, J., Wang, J., Liao, H., Wang, Q., Zhang, Q., 2018. Impacts of biogenic and anthropogenic emissions on summertime ozone formation in the Guanzhong Basin, China. *Atmos. Chem. Phys.* 18, 7489–7507. <https://doi.org/10.5194/acp-18-7489-2018>.
- Lipsky, E.M., Robinson, A.L., 2006. Effects of dilution on fine particle mass and partitioning of semivolatile organics in diesel exhaust and wood smoke. *Environ. Sci. Technol.* 40, 155–162. <https://doi.org/10.1021/es050319p>.
- Liu, S.C., Cox, R.A., Crutzen, P.J., Ehhalt, D.H., Guicherit, R., Hofzumahaus, A., Kley, D., Penkett, S.A., Phillips, L.F., Poppe, D., Rowland, F.S., 1988. Group report: oxidizing capacity of the atmosphere. In: Rowland, F.S., Isaksen, I.S.A. (Eds.), *The Changing Atmosphere*, pp. 219–232 Chichester, UK.
- Liu, J., Wang, L., Li, M., Liao, Z., Sun, Y., Song, T., Gao, W., Wang, Y., Li, Y., Ji, D., Hu, B., Kermani, V.-M., Wang, Y., Kulmala, M., 2019a. Quantifying the impact of synoptic circulation patterns on ozone variability in northern China from April to October 2013–2017. *Atmos. Chem. Phys.* 19, 14477–14492. <https://doi.org/10.5194/acp-19-14477-2019>.
- Liu, L., Wu, J., Liu, S., Li, X., Zhou, J., Feng, T., Qian, Y., Cao, J., Tie, X., Li, G., 2019b. Effects of organic coating on the nitrate formation by suppressing the N₂O₅ heterogeneous hydrolysis: a case study during wintertime in Beijing-Tianjin-Hebei (BTH). *Atmos. Chem. Phys.* 19, 8189–8207. <https://doi.org/10.5194/acp-19-8189-2019>.

- Lu, X., Hong, J., Zhang, L., Cooper, O.R., Schultz, M.G., Xu, X., Wang, T., Gao, M., Zhao, Y., Zhang, Y., 2018. Severe surface ozone pollution in China: a global perspective. *Environ. Sci. Technol. Lett.* 5, 487–494. <https://doi.org/10.1021/acs.estlett.8b00366>.
- Ma, Z., Xu, J., Quan, W., Zhang, Z., Lin, W., Xu, X., 2016. Significant increase of surface ozone at a rural site, north of eastern China. *Atmos. Chem. Phys.* 16, 3969–3977. <https://doi.org/10.5194/acp-16-3969-2016>.
- Nenes, A., Pandis, S.N., Pilinis, C., 1998. ISORROPIA: a new thermodynamic equilibrium model for multiphase multicomponent inorganic aerosols. *Aquat. Geochem.* 4, 123–152. <https://doi.org/10.1023/A:1009604003981>.
- Odum, J.R., Hoffmann, T., Bowman, F., 1996. Gas/particle partitioning and secondary organic aerosol yields. *Environ. Sci. Technol.* 30, 2580–2585. <https://doi.org/10.1021/es950943>.
- Pankow, J.F., 1994. An absorption model of gas/particle partitioning of organic compounds in the atmosphere. *Atmos. Environ.* 28, 185–188. [https://doi.org/10.1016/1352-2310\(94\)90093-0](https://doi.org/10.1016/1352-2310(94)90093-0).
- Ren, X., Brune, W.H., Olinger, A., Metcalf, A.R., Simpas, J.B., Shirley, T., Schwab, J.J., Bai, C., Roychowdhury, U., Li, Y., Cai, C., Demerjian, K.L., He, Y., Zhou, X., Gao, H., Hou, J., 2006. OH, HO₂, and OH reactivity during the PMTACS-NY Whiteface Mountain 2002 campaign: observations and model comparison. *J. Geophys. Res.* 111, D10S03. <https://doi.org/10.1029/2005JD006126>.
- Robinson, A.L., Donahue, N.M., Shrivastava, M.K., Weitkamp, E.A., Sage, A.M., Grieshop, A.P., Lane, T.E., Pierce, J.R., Pandis, S.N., 2007. Rethinking organic aerosols: semivolatile emissions and photochemical aging. *Science* 315, 1259–1262. <https://doi.org/10.1126/science.1133061>.
- Rohrer, F., Lu, K., Hofzumahaus, A., Bohn, B., Brauers, T., Chang, C.-C., Fuchs, H., Häseler, R., Holland, F., Hu, M., Kita, K., Kondo, Y., Li, X., Lou, S., Oebel, A., Shao, M., Zeng, L., Zhu, T., Zhang, Y., Wahner, A., 2014. Maximum efficiency in the hydroxyl-radical-based self-cleansing of the troposphere. *Nat. Geosci.* 7, 559–563. <https://doi.org/10.1038/ngeo2199>.
- Sarwar, G., Simon, H., Fahey, K., Mathur, R., Goliff, W.S., Stockwell, W.R., 2014. Impact of sulfur dioxide oxidation by Stabilized Criegee Intermediate on sulfate. *Atmos. Environ.* 85, 204–214. <https://doi.org/10.1016/j.atmosenv.2013.12.013>.
- Seinfeld, J.H., Pandis, S.N., 2006. *Atmospheric Chemistry and Physics - From Air Pollution to Climate Change*. 2nd ed. John Wiley & Sons, New Jersey.
- Sheehy, P.M., Volkamer, R., Molina, L.T., Molina, M.J., 2010. Oxidative capacity of the Mexico City atmosphere – part 2: a ROx radical cycling perspective. *Atmos. Chem. Phys.* 10, 6993–7008. <https://doi.org/10.5194/acp-10-6993-2010>.
- Shrivastava, M.K., Lane, T.E., Donahue, N.M., Pandis, S.N., Robinson, A.L., 2008. Effects of gas particle partitioning and aging of primary emissions on urban and regional organic aerosol concentrations. *J. Geophys. Res.* 113, D18301–D18316. <https://doi.org/10.1029/2007JD009735>.
- Stein, A.F., Saylor, R.D., 2012. Sensitivities of sulfate aerosol formation and oxidation pathways on the chemical mechanism employed in simulations. *Atmos. Chem. Phys.* 12, 8567–8574. <https://doi.org/10.5194/acp-12-8567-2012>.
- Stone, D., Whalley, L.K., Heard, D.E., 2012. Tropospheric OH and HO₂ radicals: field measurements and model comparisons. *Chem. Soc. Rev.* 41, 6348–6404. <https://doi.org/10.1039/c2cs35140d>.
- Sun, L., Xue, L., Wang, T., Gao, J., Ding, A., Cooper, O.R., Lin, M., Xu, P., Wang, Z., Wang, X., Wen, L., Zhu, Y., Chen, T., Yang, L., Wang, Y., Chen, J., Wang, W., 2016. Significant increase of summertime ozone at Mount Tai in Central Eastern China. *Atmos. Chem. Phys.* 16, 10637–10650. <https://doi.org/10.5194/acp-16-10637-2016>.
- Tan, Z., Fuchs, H., Lu, K., Hofzumahaus, A., Bohn, B., Broch, S., Dong, H., Gomm, S., Häseler, R., He, L., Holland, F., Li, X., Liu, Y., Lu, S., Rohrer, F., Shao, M., Wang, B., Wang, M., Wu, Y., Zeng, L., Zhang, Y., Wahner, A., Zhang, Y., 2017. Radical chemistry at a rural site (Wangdu) in the North China Plain: observation and model calculations of OH, HO₂ and RO₂ radicals. *Atmos. Chem. Phys.* 17, 663–690. <https://doi.org/10.5194/acp-17-663-2017>.
- Tie, X., Madronich, S., Walters, S., Zhang, R., Rasch, P., Collins, W., 2003. Effect of clouds on photolysis and oxidants in the troposphere. *J. Geophys. Res.* 108, 4642. <https://doi.org/10.1029/2003JD003659>.
- Tie, X., Huang, R.-J., Dai, W., Cao, J., Long, X., Su, X., Zhao, S., Wang, Q., Li, G., 2016. Effect of heavy haze and aerosol pollution on rice and wheat productions in China. *Sci. Rep.* 6 (1). <https://doi.org/10.1038/srep29612>.
- Tsimpidi, A.P., Karydis, V.A., Zavala, M., 2010. Evaluation of the volatility basis-set approach for the simulation of organic aerosol formation in the Mexico City metropolitan area. *Atmos. Chem. Phys.* 10, 525–546. <https://doi.org/10.5194/acp-10-525-2010>.
- Volkamer, R., San Martini, F., Molina, L.T., Salcedo, D., Jimenez, J.L., Molina, M.J., 2007. A missing sink for gas-phase glyoxal in Mexico City: formation of secondary organic aerosol. *Geophys. Res. Lett.* 34, L19807. <https://doi.org/10.1029/2007GL030752>.
- Wang, D., Zhou, Bin, Fu, Q., Zhao, Q., Zhang, Q., Chen, J., Yang, X., Duan, Y., Li, J., 2016. Intense secondary aerosol formation due to strong atmospheric photochemical reactions in summer: observations at a rural site in eastern Yangtze River Delta of China. *Sci. Total Environ.* 571, 1454–1466. <https://doi.org/10.1016/j.scitotenv.2016.06.212>.
- Wesely, M.L., 1989. Parameterization of surface resistances to gaseous dry deposition in regional-scale numerical models. *Atmos. Environ.* 23, 1293–1304. [https://doi.org/10.1016/0004-6981\(89\)90153-4](https://doi.org/10.1016/0004-6981(89)90153-4) (1967).
- Willmott, C.J., 1981. On the validation of models. *Phys. Geogr.* 2, 184–194. <https://doi.org/10.1080/02723646.1981.10642213>.
- Ying, Q., Cureño, I.V., Chen, G., Ali, S., Zhang, H., Malloy, M., Bravo, H.A., Sosa, R., 2014. Impacts of Stabilized Criegee Intermediates, surface uptake processes and higher aromatic secondary organic aerosol yields on predicted PM2.5 concentrations in the Mexico City Metropolitan Zone. *Atmos. Environ.* 94, 438–447. <https://doi.org/10.1016/j.atmosenv.2014.05.056>.
- Zhang, Q., Streets, D.G., Carmichael, G.R., 2009. Asian emissions in 2006 for the NASA INTEX-B mission. *Atmos. Chem. Phys.* 9, 5131–5153. <https://doi.org/10.5194/acp-9-5131-2009>.
- Zhao, J., Levitt, N.P., Zhang, R., Chen, J., 2006. Heterogeneous reactions of methylglyoxal in acidic media: implications for secondary organic aerosol formation. *Environ. Sci. Technol.* 40, 7682–7687. <https://doi.org/10.1021/es060610k>.
- Zhao, S., Tie, X., Cao, J., Zhang, Q., 2015. Impacts of mountains on black carbon aerosol under different synoptic meteorology conditions in the Guanzhong region, China. *Atmos. Res.* 164–165, 286–296. <https://doi.org/10.1016/j.atmosres.2015.05.016>.
- Zhou, X., Bei, N., Liu, H., Cao, J., Xing, L., Lei, W., Molina, L.T., Li, G., 2017. Aerosol effects on the development of cumulus clouds over the Tibetan Plateau. *Atmos. Chem. Phys.* 17, 7423–7434. <https://doi.org/10.5194/acp-17-7423-2017>.